Nuclear equation of state at high density and the properties of neutron stars

P. K. Sahu
Division of Physics, Graduate School of Science, Hokkaido University, Sapporo 060-0810, Japan
(Received 27 December 1999; published 6 September 2000)

We discuss the relativistic nuclear equation of state (EOS) using a relativistic transport model in heavy-ion collisions. From the baryon flow for Au + Au systems at SIS to AGS energies and above we find that the strength of the vector potential has to be reduced moderately at high density or at high relative momenta to describe the flow data at (1–10)*A* GeV. We use the same dynamical model to calculate the nuclear EOS and then employ this to calculate the gross structure of a neutron star considering the core to be composed of neutrons with an admixture of protons, electrons, muons, sigmas, and lambdas at zero temperature. We then discuss these gross properties of neutron stars such as maximum mass and radius in contrast to the observational values.

PACS number(s): 26.60.+c, 21.65.+f, 24.10.Jv, 25.75.−q

I. INTRODUCTION

The nuclear equation of state (EOS) at high density is still an unresolved issue though many theoretical and experimental efforts have been made in the last two decades to address this question in a more systematic way. Theoretically, especially in astrophysics, the density of the core inside compact objects like neutron stars is greater than the normal nuclear matter density, composed of many nonstrange and strange degrees of freedom. One of the most important characteristic features of a neutron star is its maximum allowed mass. The determination of the maximum mass and radius of neutron stars is dominated by the interactions between particles at high density and its EOS. There are many models available in the literature to deal with the maximum masses of neutron stars. These are relativistic and nonrelativistic approaches. Nonrelativistic models [1,2] based on the potential approach describe the nuclear structure for light nuclei. However, relativistic models [3–7] constructed from the Lagrangian approach explain the nuclear structure data for heavy nuclei without violating the properties of nuclear matter at the saturation density. In both conventional approaches in neutron star matter, the estimated maximum masses of neutron stars are above $2M_{\odot}$. Recently, from several calculations, it has been pointed out [8–10] that the nuclear EOS should be soft at high density. This is due to fact that all measured neutron star masses are less than $2M_{\odot}$ [11]. Various scenarios including a reduced strength of the vector field, the presence of hyperons, and the possibility of kaon condensation have been proposed to soften the EOS.

Regarding the composition of neutron star matter, there are calculations [12] which include kaons as the strange particles along with neutrons and protons, e.g., the possibility of kaon condensation. Also there are models [5,6] of neutron star matter where the composition of particles is of sigmas and lambdas as strange particles besides neutrons, protons, and electrons as nonstrange particles. Both these proposed models of neutron star matter lead to a soft EOS at high density. In this paper we consider the existence of hyperons in neutron star matter with recent compiled information of nuclear interactions from heavy-ion collisions.

Experimentally, the nuclear EOS is very important to understand nonequilibrium complicated heavy-ion collision data at very high energies. Very recently [13,14], heavy-ion collisions data such as sideward and elliptic flow have been measured at AGS energies. The sideward flow data are mainly determined by the nature of the nuclear force in the nuclear EOS. Moreover, the nuclear EOS can be understood better from elliptic flow than sideward flow, because elliptic flow has a less uncertain role in opposing streams of matter moving past each other within the reaction plane in heavy-ion collisions. Recently, the beam energy dependence of flow data [13,14] has indicated that the nuclear EOS is rather soft to lead to a possible phase transition to quark gluon plasma at high density and hence the strength of the repulsive vector potential must be low to describe these data in heavy-ion collisions.

In the present discussion, we use an extended version of relativistic mean field model [15] including momenta-dependent forces, which are taken into account phenomenologically in the relativistic transport model in heavy-ion collisions. We calculate the nuclear EOS by using the same dynamic momentum dependence constraints in the nuclear potentials and then apply them to the neutron star structure calculations. The aim of this paper is to derive the nuclear force from heavy-ion collision data, e.g., from nucleon flow data, and then to study this force on the gross structure of neutron stars by giving less importance to the composition of neutron star matter. As far as strange particles are concerned, we take minimum strange particles (Σ and Λ) in the neutron star matter calculation at high densities.

The paper is organized as follows: In Sec. II we briefly describe the relativistic nuclear EOS and its derivation from heavy-ion reactions. In Sec. III we employ the same nuclear EOS to the neutron star structure with systematic results. The conclusion and summary are presented in Sec. IV.

II. RELATIVISTIC NUCLEAR EQUATION OF STATE

Relativistic mean-field theory is a very successful model in the relativistic transport model of heavy-ion collisions as well as of nuclear structure physics. Originally, Serot and Walecka [3] proposed the relativistic mean-field model and later a modified version of this has been used widely to cal-

culate nuclear structure and nuclear matter properties. An extended version of the Serot-Walecka model, the so-called nonlinear relativistic mean-field model [4,6], has an interaction of Dirac nucleons with scalar and vector mesons as well as a nonlinear self-interaction of the scalar field. The extra nonlinear self-interaction scalar field helps to get the empirical values of the bulk properties of nuclear matter at saturation density, e.g., the nuclear incompressibility and the value of effective nucleon mass in the desirable range. The physics behind this phenomenologically successful model is that the nucleon-nucleon interaction in the mean-field theory contains strong attractive Lorentz scalar and repulsive Lorentz vector components, which almost cancel for low momenta, but produce a strong spin-orbit force consistent with the observed single-particle spectra. In the original Serot-Walecka model [3], the vector potential increases linearly with density, whereas the scalar potential changes nonlinearly. This is because the vector and scalar potentials have linear and nonlinear functions of density, respectively. However, from heavy-ion collisions data, we find that the vector potential also should have a nonlinear function of the baryon density; i.e., the strength of the vector potential should be low at high density [15] compared to the original model [3]. Recently, this fact has been taken into account by adding the nonlinear vector meson terms in the original Lagrangian density and applied to nuclear matter, neutron star matter [10], and nuclear structure [16] calculations. In our calculation, we take the nonlinear effect in the vector meson with density by employing the phenomenological momentum dependent cutoff to the vector potential term. We adopt this method, keeping in mind to describe heavy-ion reaction data at high energies, which generates a nuclear-matter-like situation in the laboratory. We recall that the mean-field energy density for nuclear matter in the relativistic mean-field model can be written as [4]

$$\varepsilon(m^*,n_b)=g_v V_0 n_b-\frac{1}{2}m_v^2V_0^2+\frac{m_s^2}{2g_s^2}(m-m^*)^2+\frac{B}{3g_s^3}(m-m^*)^3+\frac{C}{4g_s^4}(m-m^*)^4+\gamma\int_0^{k_f}\frac{d^3p}{(2\pi)^3}\sqrt{(p^2+m^*)}, \quad (1)$$

where $m^*=m-g_sS_0$ is the effective nucleon mass, n_b is the baryon density, and the spin and isospin degeneracy is $\gamma=4$. Here S_0 and V_0 are the scalar and vector fields with mass m_s and m_v, which couple to nucleons with coupling constants g_s and g_v, respectively. B and C are constant parameters describing the scalar self-interaction field and p is the nucleon momentum integrated up to the Fermi momentum k_f. In Eq. (1), the vector and scalar potentials depend on the density; however, the vector potential increases linearly with density (n_B). The parameters g_v, g_s, B, and C in Eq. (1) are determined by fitting the saturation density, binding energy, effective nucleon mass, and compression modulus at the nuclear matter density (cf. the NL3 parameter set from Table I in Ref. [4]).

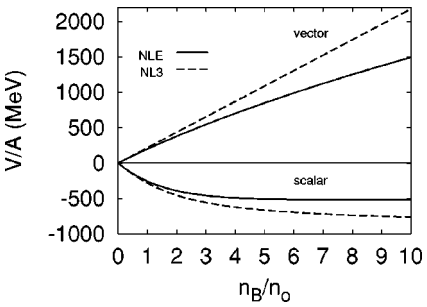

FIG. 1. Potential energy per nucleon vs baryon density in units of n_0. The solid lines (NLE) are momentum-dependent potentials and the dashed lines (NL3) are without momentum-dependent potentials (see the text).

In our present calculation, we have extended Eq. (1) to include a nonlinear dependence of the vector potential on the baryon density by implementing the momentum- (p-) dependent form factor at the vertices and can be written as [15]

$$V_0(p)=V_0\frac{p^2-\Lambda_{v1}^2}{p^2+\Lambda_{v2}^2}, \quad (2)$$

where the cutoff parameters $\Lambda_{v1}=0.37$ GeV, $\Lambda_{v2}=0.9$ GeV, and V_0 is the vector potential. For completeness, we incorporate the momentum-dependent form factor at the scalar vertices in a form given as [15]

$$V_s(p)=V_s\frac{p^2-\Lambda_{s1}^2}{p^2+\Lambda_{s2}^2}, \quad (3)$$

where the cutoff parameters $\Lambda_{s1}=0.71$ GeV, $\Lambda_{s2}=1.0$ GeV, and the V_s is scalar potential. The choice of these form factors is similar to that used in effective meson-exchange interactions for nucleon-nucleon scattering [17] and later this strategy was used in a relativistic approach for nucleus-nucleus collisions from SIS to SPS energies [18]. The values of the cutoff parameters in vector and scalar vertices are chosen to describe properly the Schrödinger-equivalent potential until 1 GeV and the flow data at AGS energies. These cutoff parameters are not unique for various types of equations of state to fit the Schrödinger-equivalent potential until 1 GeV and the flow data at AGS energies simultaneously. We note that the form factor, Eq. (2), will make the vector interaction weak at high baryon density and at high energies in heavy-ion collisions. At these energies, it has also been observed that the strength of the repulsive vector potential should be reduced considerably at high density or at high relative momenta to describe the flow data. Theoretically, it is important to understand the decrease of vector coupling at high density. In contrast to heavy-ion reactions, in this line some works have been performed [19] and more are required to obtain the details [20].

We show in Fig. 1, the scalar and vector potential energies as a function of baryon density. The solid lines (NLE

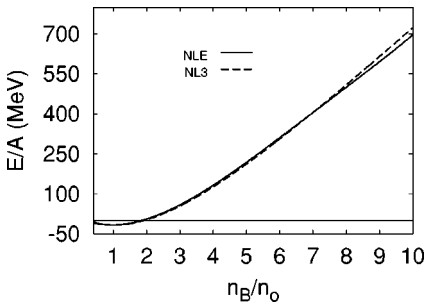

FIG. 2. Energy per nucleon vs baryon density in units of n_0. The models are the same as in Fig. 1.

curves) are associated with the momentum-dependent form factors given in Eqs. (2) and (3) that describe the flow data best from SIS to AGS energies. The dashed lines (NL3 curves) are without momentum-dependent potentials. The vector part for NLE is substantially low at high baryon density as that of the NL3 parameter set. At high density the reduction of the vector potential is more significant than the scalar potential for NLE curves. Therefore, the net effect of changed potentials is the vector potential due to a substantial reduction of the vector part at high baryon density. For example, at $\rho=8\rho_0$, the values of the vector part and scalar part are 1250 MeV and -511 MeV, respectively, for NLE, where the value of vector part is 1740 MeV and scalar part is -735 MeV for NL3. So the net reduction is dominated by the vector potential in the NLE model. The corresponding EOS versus baryon density is shown in Fig. 2 for the extended momentum-dependent model (NLE) as well as the original nonlinear model (NL3). NLE has the momentum-dependent form factor in the vector and scalar potentials. The other nuclear EOS has been discussed in more detail in Ref. [6] by varying the nuclear incompressibility from low (soft) 250 MeV to high (stiff) 350 MeV values. We do not elaborate on that issue here, because we would like to emphasize more the momentum-dependent force in the nuclear EOS along the line of heavy-ion reaction data. We see in Fig. 2 that the NLE nuclear EOS is softer than NL3 at density $\geqslant 7\rho_0$ and is slightly stiffer at density $\leqslant 7\rho_0$. The incompressibility is close (~ 380 MeV) to the NL3 value at saturation density. In the next section, we would like to implement this model in neutron star matter, where the core density is in the range of $>(5-8)\rho_0$. So in the present model, the stiffness of the equation of state changes around that density, due to the main contribution coming from the reduced vector potential. However, in the heavy-ion flow calculation at AGS energies, the stiffness of the equation of state not only comes from the net reduction of the vector potential but also from the transition from hadrons to string degrees of freedom as discussed in our recent work [15]. It has been pointed out recently [21] from a simulation calculation that one might even reach $10\rho_0$, although only for a very short time of a few fm/c at the energy range between AGS and SPS energies. Hence at the AGS energy range, the baryon density is expected to reach more than $>5\rho_0$.

Recently, elliptic flow and sideward flow have been studied theoretically with increasing beam energy by various types of equations of state and possible signature of the phase transition [22]. More precisely, the beam energy dependence of the observed elliptic flow has been interpreted as such a possible phase transition. The reason is that a simulation model including different kinds of equations of state is consistent with a softening of the equation of state. This softening of the equation of state can be realized in many ways, for example, (i) by reducing the strong repulsive force in the equation of state with the help of a momentum-dependent form factor and fitting it with a Schrödinger-equivalent potential and (ii) by implementing the transition from hadronic to string degrees of freedom with beam energies in the simulation model [15]. In our calculation, we implement the former one, where the thermodynamic pressure in the extended model NLE is lower as compared to the NL3 model due to a less repulsive force at the AGS energy regime. We thus get reduced repulsive force because of the strong cutoff parameters, Eq. (2), in the vector potential. Also this cutoff makes the vector potential a nonlinear function of the baryon density.

III. NEUTRON STAR MATTER AND PROPERTIES OF NEUTRON STAR

A. Neutron star matter

The core of the neutron star plays a significant role to determine gross structural properties like the maximum mass and radius of the neutron star. The density of the core inside the neutron star is greater than the normal nuclear matter density and hence nuclear interactions are important in the construction of the neutron star matter EOS around that density. Moreover, in such a high density, strange particles are expected to be present along with the usual neutron matter like neutrons, protons, and electrons. So in our neutron star matter calculation we assume that the core of neutron star matter is composed of neutrons with an admixture of protons, electrons, muons, and hyperons (Λ and Σ^-) [6]. The concentrations of each particle can be determined by using the condition of equilibrium under weak interactions (assuming that neutrinos are not degenerate) and electric charge neutrality:

$$\mu_p=\mu_n-\mu_e, \quad \mu_\Lambda=\mu_n,$$

$$\mu_{\Sigma^-}=\mu_n+\mu_e, \quad \mu_\mu=\mu_e,$$

$$n_p=n_e+n_\mu+n_{\Sigma^-}. \tag{4}$$

In addition, the total baryon density is $n_B=n_n+n_p+n_\Lambda+n_{\Sigma^-}$ and the baryon chemical potential is $\mu_B=\mu_n$, where n_i and μ_i stand for number density and chemical potential for the ith particle, respectively.

Since the nuclear force is known to favor isospin symmetry and the symmetry energy arising solely from the Fermi energy is known to be inadequate to account for the empirical value of the symmetry energy (~ 32 MeV), we include the interaction due to the isospin triplet ρ meson in the relativistic nonlinear mean-field model for the purpose of de-

scribing neutron-rich matter [7]. It is noted that the ρ meson will contribute a term $=(g_\rho^2/8m_\rho^2)(n_p-n_n)^2$ to the energy density and pressure in absence of hyperons. We fix the coupling constant g_ρ by requiring that the symmetric energy coefficient correspond to the empirical value 32 MeV. Then the neutron star matter EOS is calculated from the energy density ε and pressure P, which are given as follows [6]:

$$\varepsilon=\frac{1}{2}m_v^2V_0^2+\frac{1}{2}m_\rho^2\rho_0^2+\frac{1}{2}m_s^2S_0^2+\frac{B}{3}S_0^3+\frac{C}{4}S_0^4+\sum_i \varepsilon_{FG}+\sum_l \varepsilon_{FG},$$

$$P=\frac{1}{2}m_v^2V_0^2+\frac{1}{2}m_\rho^2\rho_0^2-\frac{1}{2}m_s^2S_0^2-\frac{B}{3}S_0^3-\frac{C}{4}S_0^4+\sum_i P_{FG}+\sum_l P_{FG}, \quad (5)$$

where ρ_0 is the third component in isospin space. In the above equations ε_{FG} and P_{FG} are the relativistic noninteracting energy density and pressure of the baryons (i) and leptons (l), respectively.

The three coupling constant parameters of the hyperon-meson interaction are not well known. Therefore, we fix the ratio of the hyperon-meson and nucleon-meson couplings for σ, ω, and ρ mesons, respectively, (i) by staying very close to the quark counting rule [6]—e.g., the potentials seen by Λ and Σ in nuclear matter are ~ -30 MeV [23]—and (ii) assuming the attractive potential seen by Λ and the repulsive potential seen by Σ to be ~ -30 MeV [23] and $\sim +10$ MeV [9,24,25], respectively, at nuclear matter density. An analysis of various experimental data on hypernuclei [23–26] suggests that the strength of the Σ potential may be either repulsive or attractive at nuclear matter density. This point will be cleared further after an analysis of more hypernuclei data in the near future and the general discussions are given in the recent reference [27]. Because of this fact, we consider the two possibilities of strength of the Σ potential as discussed above.

Taking all these parameters into Eqs. (4), we show the concentration of particles ($x_i=n_i/n_B$, $i=p$, Σ, and Λ) versus baryon density for NLE1, NLE2, and NL3 models in Fig. 3. We display p, Σ, and Λ particles in this figure due to the practical importance to neutron stars; for example, the p fraction plays a role for the cooling process of neutron stars and the order of appearance of strange particles with density may influence the EOS of neutron star matter. In NLE1 and NL3 models, the potentials for Λ and Σ are taken to be equal to ~ -30 MeV, where the potentials for Λ and Σ are chosen to be ~ -30 MeV and $\sim +10$ MeV, respectively, in the NLE2 model. However, the momentum-dependent cutoff to the vector potential is incorporated in both NLE1 and NLE2 models. We notice in Fig. 3 that the concentration of particles like Σ^- and Λ starts appearing after 2 times the nuclear matter density for all models. In NLE1 and NL3 models, the order of appearance of strange particles (first Σ and then Λ) is the same due to the equal strength of the potential felt by strange particles. Where the situation is quite different in the case of the NLE2 model, here Λ appears first around >2.5 times the nuclear matter density and Σ^- starts coming much later [9] around >3.5 times the nuclear matter density. This is due to the fact that Σ sees extra strength, $+40$ MeV, of the potential than the Λ potential, which is repulsive. In both NLE1 and NLE2 models, the strange particles start coming slightly later than NL3, due to a reduction of the vector potential by the momentum-dependent cutoff as given in Eq. (2). However, the change of proton concentration is not very significant with density for all models, except a slight decreasing tendency at high density was shown by NLE2. At around 1.5 times nuclear matter density, the value of the proton concentration crosses the threshold value 0.11 (horizontal line in Fig. 3), which shows that a direct URCA process can possibly lead to a cooling of neutron stars in all models [28].

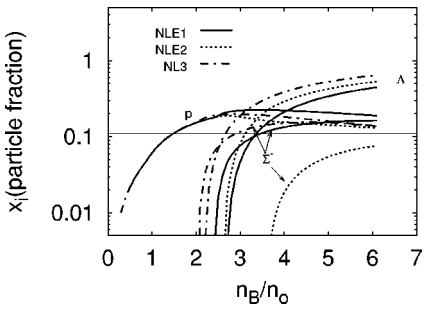

FIG. 3. The concentration of each particle ($x_i=n_i/n_B$) vs baryon density in units of n_0. The momentum-dependent potentials have been incorporated in NLE1 (solid line) and NLE2 (dashed line). The dash-dotted lines (NL3) are without momentum-dependent potentials. The potentials seen by Λ and Σ are the same in NLE1 and NL3 (dash-dotted line) and are different in NLE2 (see text).

B. Maximum mass and radius of neutron stars

The gross structure of neutron stars such as mass and radius calculated from equations that describe the hydrostatic equilibrium of degenerate stars without rotation in general relativity is called the Tolman-Oppenheimer-Volkoff (TOV) equations [7]. From the dynamics and transport properties of pulsars, the additional structure parameters of neutron stars like the moment of inertia I and the surface redshift $z=1/\sqrt{1-2GM/Rc^2}-1$ are important and are given more elaborately in Ref. [7].

We solve the TOV equations by constructing the EOS for the entire density region starting from the higher density at the center to the surface density. The composite EOS for the entire neutron star density span was constructed by joining the NLE and NL3 neutron star matter EOS to the EOS of the density range (i) 10^{14}–5×10^{10} g cm^{-3} [29], (ii) 5×10^{10}–10^3 g cm^{-3} [30], and (iii) less than 10^3 g cm^{-3} [31]. The composite neutron star matter EOS are plotted in Fig. 4 for NLE1, NLE2, and NL3 models, which are used to

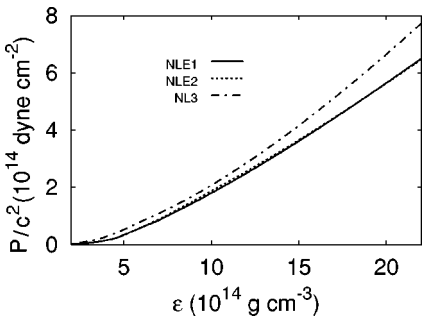

FIG. 4. The neutron star matter pressure vs energy density. The models are the same as in Fig. 3.

calculate the neutron star structures as discussed above. From Fig. 4 we find that the pressure is low at high density for the NLE1 and NLE2 EOS and hence the soft EOS compared to the NL3 EOS. If we look at Fig. 3, the order of appearance of Λ particles with density is reflected in the same order of the nature of the EOS. That is, NL3 is stiffer than the NLE1 and NLE2 EOS, because the momentum-dependent form factor in the latter two models has reduced the vector potential at high density. So NLE2 is similar to the NLE1 EOS, except for being slightly stiffer than NLE1 due to the strong repulsive potential present in Σ particles as can be seen in Fig. 4. We also notice in Fig. 4 that the NLE2 EOS does not change significantly on the choice of the repulsive Σ potential in contrast to the NLE1 EOS.

The predicted maximum neutron star masses are very close to the observational values for the NLE1 and NLE2 EOS. The results for the neutron star structure parameters are tabulated in Table I and the central density versus mass is plotted in Fig. 5. From Fig. 5 and Table I, we observe that the maximum masses of the stable neutron stars are $2.18M_{\odot}$, $1.94M_{\odot}$, and $1.97M_{\odot}$ and the corresponding radii are 11.9, 10.7, and 10.8 km for the NL3, NLE1, and NLE2 EOS, respectively. The corresponding central densities are 2.0×10^{15}, 2.2×10^{15}, and 2.2×10^{15} g cm^{-3} (>7 times nuclear matter density) for NL3, NLE1, and NLE2, respectively, at the maximum neutron star masses. These maximum masses calculated in our models are in the range of recent observations [32–35], where the observational consequences are discussed below. Very recently, it has been observed that the best determined neutron star masses [11] are found in binary pulsars and all lie in the range $(1.35\pm0.04)M_{\odot}$ except for the nonrelativistic pulsars PSR J1012+5307 of mass $M=(2.1\pm0.8)M_{\odot}$ [32]. There are several x-ray binary masses that have been measured, the heaviest among them being Vela X-1 with $M=(1.9\pm0.2)M_{\odot}$ [33] and Cygnus X-2 with $M=(1.8\pm0.4)M_{\odot}$ [34]. From the recent discovery of high-frequency brightness oscillations in low-mass x-ray binaries, the large mass of the neutron star in QPO4U of $1820-30(M=2.3)M_{\odot}$ [35] is confirmed and this provides a new method to determine the masses and radii of neutron stars. We also tabulate the moment of inertia and the surface redshift in Table I, which are important for the dynamic and transport properties of pulsars.

TABLE I. Neutron star structure parameters.

ε_c (g cm^{-3})	R (km)	$M/M_{\odot}$	z	I (g cm^2)	
6.0×10^{14}	10.82	1.00	0.17	9.55×10^{44}	NLEI
8.0×10^{14}	11.46	1.44	0.26	1.61×10^{45}	
1.0×10^{15}	11.54	1.66	0.32	1.94×10^{45}	
1.5×10^{15}	11.27	1.89	0.41	2.15×10^{45}	
2.0×10^{15}	10.89	1.94	0.45	2.08×10^{45}	
2.5×10^{15}	10.55	1.94	0.48	1.96×10^{45}	
3.0×10^{15}	10.26	1.93	0.50	1.83×10^{45}	
4.0×10^{15}	9.83	1.88	0.51	1.62×10^{45}	
6.0×10^{14}	10.87	1.03	0.18	9.93×10^{44}	NLE2
8.0×10^{14}	11.55	1.48	0.27	1.70×10^{45}	
1.0×10^{15}	11.63	1.72	0.33	2.05×10^{45}	
1.5×10^{15}	11.36	1.92	0.41	2.24×10^{45}	
2.0×10^{15}	10.98	1.97	0.46	2.15×10^{45}	
2.5×10^{15}	10.96	1.97	0.47	2.02×10^{45}	
3.0×10^{15}	10.37	1.95	0.50	1.88×10^{45}	
4.0×10^{15}	9.92	1.89	0.51	1.66×10^{45}	
6.0×10^{14}	13.20	1.60	0.25	2.31×10^{45}	NL3
8.0×10^{14}	13.26	1.89	0.31	2.84×10^{45}	
1.0×10^{15}	13.08	2.04	0.36	3.02×10^{45}	
1.5×10^{15}	12.43	2.17	0.44	2.96×10^{45}	
2.0×10^{15}	11.85	2.18	0.48	2.72×10^{45}	
2.5×10^{15}	11.38	2.16	0.51	2.49×10^{45}	
3.0×10^{15}	11.00	2.13	0.53	2.28×10^{45}	
4.0×10^{15}	10.40	2.05	0.55	1.95×10^{45}	

At this point, we argue that the softening of the EOS may lead to kaon condensation in neutron stars [36] and hence may give a constraint on the best determined maximum mass [11]. However, we feel that from the KaoS data on kaon production, together with kaon flow from heavy-ion reactions [37], it is important to know the momentum-dependent K^+ and K^- potentials in dense matter according to the prediction of chiral perturbation theory. In the present calculation, we do not explore this, but work is in progress [38] by implementing the same momentum forces as given in Eqs. (2) and (3).

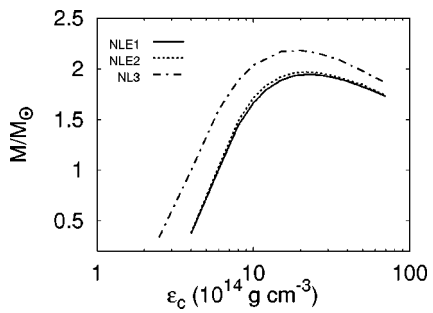

FIG. 5. The neutron star mass vs radius. The models are the same as in Fig. 3.

IV. SUMMARY

We have described the nuclear EOS in the framework of relativistic mean-field theory using a relativistic transport model of the heavy-ion collisions. From the heavy-ion collision data, more specifically, the baryon flow for Au+Au systems at SIS to AGS energies and above we noticed that the strength of the vector potential has to be reduced substantially at high density and high relative momenta to describe the experimentally observed flow data at (1–10)*A* GeV. In a different way, the vector potential should be a nonlinear function of the baryon density. We took this effect into account by introducing a momentum-dependent cutoff into the vector potential in contrast to heavy-ion collision data. We use the same dynamic treatment in our relativistic mean-field model to calculate the nuclear EOS. It is found that the derived nuclear EOS is moderately soften at density $\geqslant 7\rho_0$ than the originally considered nuclear EOS without momentum-dependent potentials. This is due to the reduction of the repulsive nuclear interaction in the nuclear EOS at high density. We then employ the same nuclear EOS to the neutron star structure calculation.

In neutron star matter, the core of the neutron stars is considered to be composed of neutrons along with an admixture of protons, electrons, muons, and hyperons at zero temperature. The resulting maximum masses of stable neutron stars are $2.18M_\odot$, $1.94M_\odot$, and $1.97M_\odot$ for the NL3, NLE1, and NLE2 models, respectively. We observed that the maximum mass of the neutron star for NLE1 and NLE2 is lower than that for NL3 due to a reduction of the vector field at higher densities. Also, we noticed that the potential felt by Σ particles is not so relevant to neutron star structure calculations. The corresponding neutron star radii are 11.9, 10.7, and 10.8 km for NL3, NLE1, and NLE2, respectively, whereas the corresponding central densities are 2.0×10^{15}, 2.2×10^{15}, and 2.2×10^{15} g cm^{-3}, respectively, for NL3, NLE1, and NLE2 at the maximum neutron star mass. We found that the maximum mass for NLE1 and NLE2 is in the observable region [32–35] $1.4M_\odot < M_{max} < 2.2M_\odot$ and the corresponding radius is between 8 and 12 km.

ACKNOWLEDGMENTS

The author would like to thank W. Cassing and A. Ohnishi for a critical reading and W. Cassing, A. Ohnishi, and Y. Akaishi for fruitful discussions. He would also like to acknowledge support from the Japan Society for the Promotion of Science, Japan.

[1] A. Akmal, V. R. Pandharipande, and D. G. Ravenhall, Phys. Rev. C **58**, 1804 (1998).
[2] R. B. Wiringa, V. Fiks, and A. Fabrocini, Phys. Rev. C **38**, 1010 (1988).
[3] B. D. Serot and J. D. Walecka, Adv. Nucl. Phys. **16**, 1 (1986).
[4] A. Lang, B. Blättel, W. Cassing, V. Koch, U. Mosel, and K. Weber, Z. Phys. A **340**, 207 (1991).
[5] N. K. Glendenning, F. Weber, and S. A. Moszkowski, Phys. Rev. C **45**, 844 (1992).
[6] S. K. Ghosh, S. C. Phatak, and P. K. Sahu, Z. Phys. A **352**, 457 (1995).
[7] P. K. Sahu, R. Basu, and B. Datta, Astrophys. J. **416**, 267 (1993).
[8] H. Heiselberg and M. Hjorth-Jensen, Astrophys. J. Lett. **525**, L45 (1999).
[9] S. Balberg and A. Gal, Nucl. Phys. **A625**, 435 (1997).
[10] H. Shen, H. Toki, K. Oyamatsu, and K. Sumiyoshi, Nucl. Phys. **A637**, 435 (1998).
[11] S. E. Thorsett and D. Chakrabarty, Astrophys. J. **512**, 288 (1999).
[12] G. Brown, C. Lee, M. Rho, and V. Thorsson, Nucl. Phys. **A572**, 693 (1994); T. Waas, M. Rho, and W. Weise, *ibid.* **A617**, 449 (1997).
[13] E895 Collaboration, H. Liu *et al.*, Nucl. Phys. **A638**, 451c (1998).
[14] E895 Collaboration, C. Pinkenburg *et al.*, Phys. Rev. Lett. **83**, 1295 (1999).
[15] P. K. Sahu, A. Hombach, W. Cassing, M. Effenberger, and U. Mosel, Nucl. Phys. **A640**, 493 (1998); P. K. Sahu, W. Cassing, U. Mosel, and A. Ohnishi, *ibid.* **A672**, 376 (2000).
[16] Y. Sugahara and H. Toki, Nucl. Phys. **A579**, 557 (1994).
[17] R. Machleidt, K. Holinde, and Ch. Elster, Phys. Rep. **149**, 1 (1987).
[18] W. Ehehalt and W. Cassing, Nucl. Phys. **A602**, 449 (1996).
[19] C. Song, G. E. Brown, D. Min, and M. Rho, Phys. Rev. C **56**, 2244 (1997); Y. Kim and H. K. Lee, Phys. Rev. C **62**, 037901 (2000); Y. Kim, R. Rapp, G. E. Brown, and M. Rho, *ibid.* **62**, 015202 (2000).
[20] P. K. Sahu *et al.* (unpublished).
[21] B. Friman *et al.*, nucl-th/9711065; E. L. Bratkovskaya and W. Cassing, Nucl. Phys. **A619**, 413 (1997).
[22] E895 Collaboration, H. Liu *et al.*, Phys. Rev. Lett. **84**, 5488 (2000); J. Stachel, Nucl. Phys. **A654**, 119 (1999).
[23] R. E. Chrien and C. B. Dover, Annu. Rev. Nucl. Part. Sci. **39**, 227 (1989).
[24] Y. Yamamoto, S. Nishizaki, and T. Takatsuka (unpublished).
[25] J. Dabrowski, Phys. Rev. C **60**, 025205 (1999).
[26] T. Harada and Y. Akaishi, Phys. Lett. B **262**, 205 (1991).
[27] T. A. Rijken, V. G. J. Stoks, and Y. Yamamoto, Phys. Rev. C **59**, 21 (1999).
[28] J. Boguta, Phys. Lett. **106B**, 255 (1981); C. J. Pethick, Rev. Mod. Phys. **64**, 1133 (1992).
[29] J. W. Negle and D. Vautherin, Nucl. Phys. **A207**, 298 (1973).
[30] G. Baym, C. J. Pethick, and P. G. Sutherland, Astrophys. J. **170**, 299 (1971).
[31] R. P. Feynmann, N. Metropolis, and E. Teller, Phys. Rev. **75**, 308 (1949).
[32] J. van Paradijs, in *The Many Faces of Neutron Stars*, edited by R. Buccheri, J. van Paradijs, and M. A. Alpar (Kluwer Academic, Dordecht, in press).
[33] O. Barziv (unpublished); M. H. van Kerkwijk, J. van Paradijs, and E. J. Zuiderwijk, Astron. Astrophys. **303**, 497 (1995) (larger uncertainties).

[34] J. A. Orosz and E. Kuulkers, Mon. Not. R. Astron. Soc. (to be published).
[35] M. C. Miller, F. K. Lamb, and P. Psaltis, Astrophys. J. **508**, 791 (1998).
[36] G. Q. Li, C.-H. Lee, and G. E. Brown, Phys. Rev. Lett. **79**, 5214 (1997).
[37] M. D. Parland *et al.*, Phys. Rev. Lett. **75**, 2100 (1995); J. Ritman *et al.*, Z. Phys. A **352**, 355 (1995); G. Agakichiev *et al.*, Phys. Rev. Lett. **75**, 1272 (1995).
[38] P. K. Sahu *et al.* (unpublished).